

RESEARCH

Open Access



# Comparison of PET tracing and biodistribution between $^{64}\text{Cu}$ -labeled micro-and nano-polystyrene in a murine inhalation model

Joycie Shanmugiah<sup>1,2</sup>, Javeria Zaheer<sup>1</sup>, Changkeun Im<sup>1,2</sup>, Choong Mo Kang<sup>1,2</sup> and Jin Su Kim<sup>1,2\*</sup>

## Abstract

**Introduction** Recent studies showed the presence of microplastic in human lungs. There remains an unmet need to identify the biodistribution of microplastic after inhalation. In this study, we traced the biodistribution of inhaled micro-sized polystyrene (mPS) and/or nano-sized PS (nPS) using  $^{64}\text{Cu}$  with PET in mice.

**Methods** We used 0.2–0.3- $\mu\text{m}$  sized mPS and 20-nm sized nPS throughout.  $^{64}\text{Cu}$ -DOTA-mPS,  $^{64}\text{Cu}$ -DOTA-nPS and/or  $^{64}\text{CuCl}_2$  were used to trace the distribution in the murine inhalation model. PET images were acquired using an INVEON PET scanner at 1, 12, 24, 48, and 72 h after intratracheal instillation, and the  $\text{SUV}_{\text{max}}$  for interesting organs were determined, biodistribution was then determined in terms of percentage injected dose/gram of tissue (%ID/g). Ex vivo tissue-radio thin-layer chromatography (Ex vivo-radioTLC) was used to demonstrate the existence of  $^{64}\text{Cu}$ -DOTA-PS in tissue.

**Results** PET image demonstrated that the amount of  $^{64}\text{Cu}$ -DOTA-mPS retained within the lung was significantly higher than  $^{64}\text{Cu}$ -DOTA-nPS until 72 h;  $\text{SUV}_{\text{max}}$  values of  $^{64}\text{Cu}$ -DOTA-mPS in lungs was  $11.7 \pm 5.0$ ,  $48.3 \pm 6.2$ ,  $65.5 \pm 2.3$ ,  $42.2 \pm 13.1$ , and  $13.2 \pm 2.3$  at 1, 12, 24, 48, and 72 h respectively whereas it was  $31.2 \pm 3.1$ ,  $17.3 \pm 5.9$ ,  $10.0 \pm 3.4$ ,  $8.1 \pm 2.4$  and  $8.9 \pm 3.6$  for  $^{64}\text{Cu}$ -DOTA-nPS at the corresponding timepoints. The biodistribution data supported the PET data with a similar pattern of clearance of the radioactivity from the lung. nPS cleared rapidly post instillation in comparison to mPS within the lungs. Higher accumulation of %ID/g for nPS (roughly 2 times) were observed compared to mPS in spleen, liver, intestine, thymus, kidney, brain, salivary gland, ovary, and urinary bladder. Ex vivo-radioTLC was used to demonstrate that the detected gamma rays originated from  $^{64}\text{Cu}$ -DOTA-mPS or nPS.

**Conclusion** PET image demonstrated the differences in accumulations of mPS and/or nPS between lungs and other interesting organs. The information provided may be used as the basis for future studies on the toxicity of mPS and/or nPS.

**Keywords** Micro-polystyrene, Nano-polystyrene,  $^{64}\text{Cu}$ , PET, Inhalation, Plastic

\*Correspondence:

Jin Su Kim

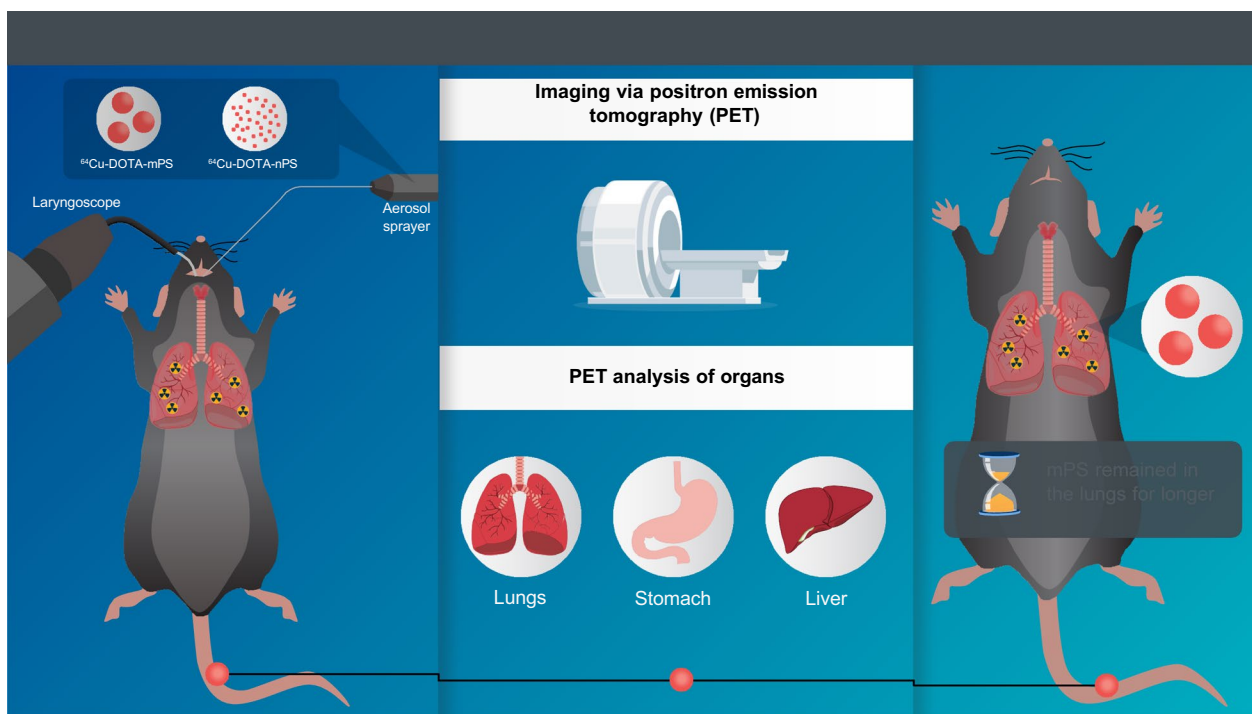
kjs@kiram.s.re.kr

Full list of author information is available at the end of the article



© The Author(s) 2024. **Open Access** This article is licensed under a Creative Commons Attribution 4.0 International License, which permits use, sharing, adaptation, distribution and reproduction in any medium or format, as long as you give appropriate credit to the original author(s) and the source, provide a link to the Creative Commons licence, and indicate if changes were made. The images or other third party material in this article are included in the article's Creative Commons licence, unless indicated otherwise in a credit line to the material. If material is not included in the article's Creative Commons licence and your intended use is not permitted by statutory regulation or exceeds the permitted use, you will need to obtain permission directly from the copyright holder. To view a copy of this licence, visit <http://creativecommons.org/licenses/by/4.0/>. The Creative Commons Public Domain Dedication waiver (<http://creativecommons.org/publicdomain/zero/1.0/>) applies to the data made available in this article, unless otherwise stated in a credit line to the data.

## Graphical abstract



## Introduction

Microplastics were subsequently found to accumulate in aquatic ecosystems and marine life [1, 2] and in the deep organs of humans [3], contributing significantly to environmental and public health concerns [4]. Living beings are constantly prone to exposure to microplastic by ingestion, and/or inhalation [5]. Several studies in which microplastic fed mouse models developed various physiological variations as well as genetic-level mutations, resulting in disorders [6–9]. Polystyrene (PS) is one of the widely used plastic for most daily-use products and we traced the biodistribution of orally administered  $^{64}\text{Cu}$ -labeled PS in mice by PET [10].

Nanoplastics with dimensions ranging from 1 to 100 nm have been observed to show adverse effects on the environment and human health [11–13]. Mechanical stress, ultraviolet radiation, and chemical degradation can result in the fragmentation of microplastic to nanoplastic. Since the size of nano-plastics are lesser than 100 nm diameter, there is high possibility that they can enter cells and disrupt the cellular activity. Hence it is important to look into the potential toxicity of nanoplastics via inhalation as well [14].

Inhalation was identified as an exposure route for microplastic when recent studies revealed deposition

of microplastics even in human lungs [3, 15]. While microplastic evidently enter the human body through diet [16–18], airborne microplastic present indoors and outdoors may also be a dominant source [19–21]. The potential harmful effects of intratracheally instilled 5- $\mu\text{m}$  microplastics were reported in the lungs of mice [22].

Until now, the translocation of microplastics such as PS from the pulmonary tissue to other organs has not been thoroughly explored. In addition, the difference of biodistribution during inhalation between micro-sized PS (mPS) and nano-sized PS (nPS) remains unclear. Figure 1 shows the schematic figure of this study. To visualize the distribution of mPS and nPS in the respiratory system, the PS were labeled with the PET radioisotope  $^{64}\text{Cu}$  and instilled directly into the trachea of mice. An aerosol sprayer was used to ensure that  $^{64}\text{Cu}$  labeled PS was distributed equally in the lungs. Then, we compared the biodistribution of PS in the respiratory system and their subsequent distribution to other parts of the body post-instillation using  $^{64}\text{Cu}$  labeled mPS and/or nPS in vivo PET, and ex vivo biodistribution for this study.

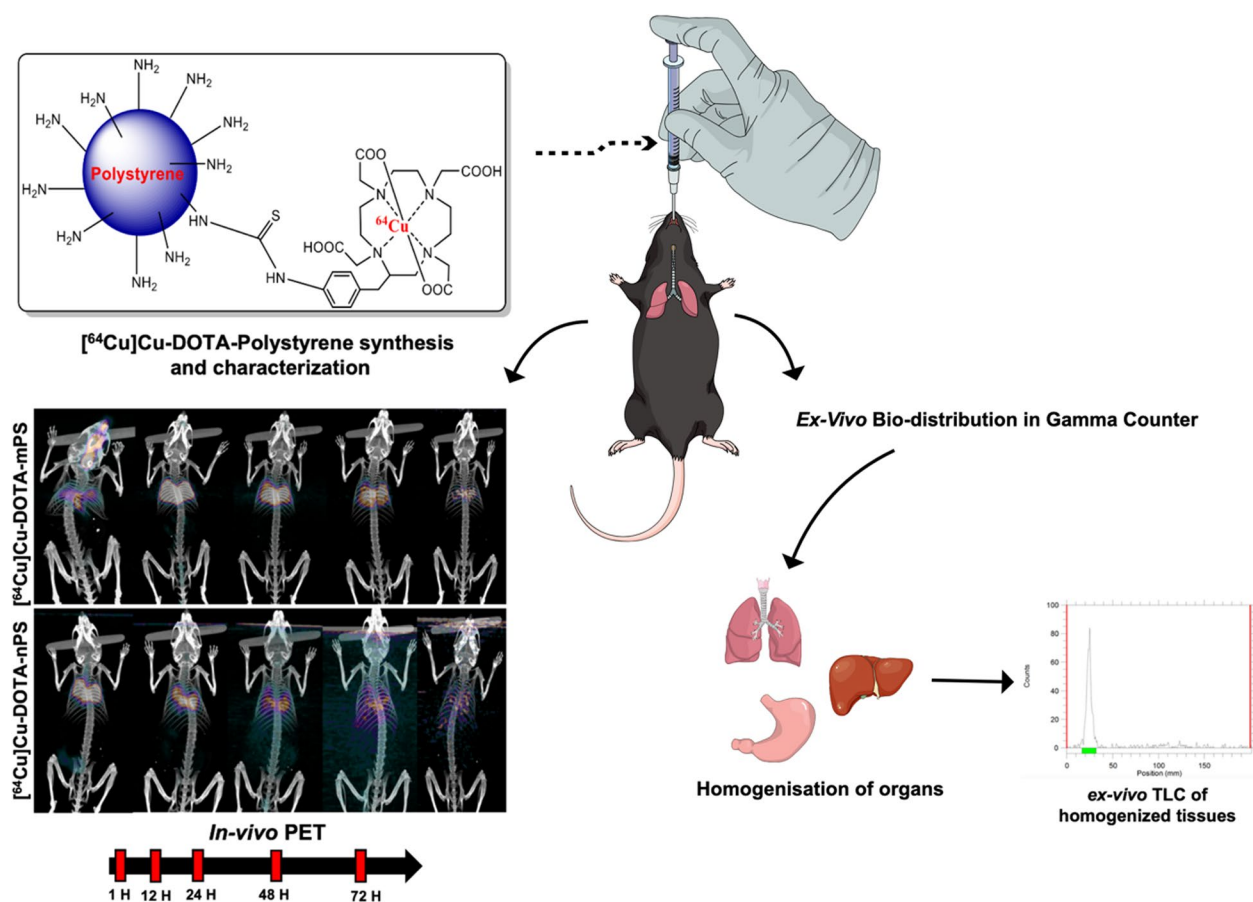


**Fig. 1** Schematic of the experiment.  $^{64}\text{Cu-DOTA-mPS/nPS}$  was synthesized and characterized using HPLC and radiochemical purity was analyzed using radio-TLC.  $^{64}\text{Cu-DOTA-mPS/nPS}$  was intra-tracheally instilled into mice and PET imaging was performed. The organs were extracted at each timepoint and radioactivity was counted in a gamma counter followed by tissue homogenization and *ex-vivo* TLC analysis to confirm the stability of the labelled products in each organ (mPS = micro polystyrene, nPS = nano polystyrene)

## Materials and methods

### Conjugation and $^{64}\text{Cu}$ labeling PS

Surface-modified mPS with particle size between 0.2–0.3  $\mu\text{m}$  was obtained commercially (Spherotech<sup>TM</sup> amino-polystyrene particles; Lake Forest, IL, USA) and conjugated with S-2-(-4-isothiocyanatobenzyl)-1,4,7,10 tetraazacyclododecane tetraacetic acid (p-SCN-Bn-DOTA; Macrocyclics<sup>TM</sup>) as previously reported by our research group [10]. Briefly, 2 mg of mPS was added to 240  $\mu\text{L}$  of 0.1 M sodium carbonate buffer (pH 9.0) along with 770  $\mu\text{g}$  of p-SCN-Bn-DOTA in 100  $\mu\text{L}$  of deionized water (Sigma-Aldrich) and incubated at 25  $^{\circ}\text{C}$  with mild shaking in a thermomixer at 1000 rpm for 20 h. The incubated mixture was purified using a Vivispin 20 centrifugal concentrator (Sartorius Stedium Biotech, USA) with a 100-kDa cut-off.

The above-mentioned procedure was also used for radiolabeling nPS with 20 nm amino-polystyrene purchased from Nanocs Inc. (New York, NY, USA). nPS was washed with deionized water containing 0.05% Tween-20

(Sigma-Aldrich, Saint Louis, MO, USA) with centrifugation in a Vivispin 20 centrifugal concentrator (10-kDa molecular weight cutoff [MWCO], Sartorius Stedium Biotech, USA) to prevent aggregation, and sonicated for 10 min before conjugation with p-SCN-Bn-DOTA. The chelator-conjugated nPS was purified in a Vivispin 20 centrifugal concentrator (10 kDa), and the final concentrations of both mPS and nPS after conjugation with p-SCN-Bn-DOTA was 2 mg/100  $\mu\text{L}$ . The number of moles of DOTA conjugated per milligram of the PS beads was determined using high-performance liquid chromatography (HPLC), and characterization of DOTA-PS was performed using the SU8010 ultra-high-resolution field emission scanning electron microscopy (FE-SEM) system.

$^{64}\text{Cu}$  produced in the cyclotron (installed in KIRAMS) was dried by argon gas purging and re-dissolved in 0.01 N HCL (9.25 MBq/ $\mu\text{L}$ ). To the conjugated mixture containing DOTA-PS, 40.7 MBq of  $^{64}\text{CuCl}_2$  was added and incubated at 40  $^{\circ}\text{C}$  for 30 min at 1000 rpm along with 80  $\mu\text{L}$

of sodium acetate buffer (pH 5.0). The radiolabeled mPS was purified using a 100-kDa MWCO centrifugal filter for 30 min at 3500 rpm. This step was repeated twice with deionized water until the final volume was reduced to less than 200  $\mu$ L. On the other hand, radiolabeled nPS was incubated with 50 mM ethylenediaminetetraacetic acid (EDTA, pH 6.0) for 15 min prior to purification using a 10-kDa MWCO centrifugal filter for 30 min at 3500 rpm and 25 °C. EDTA, which is a strong chelator, binds to free copper [23], ensuring better purification and greater radiochemical purity. The  $^{64}\text{Cu}$ -labeled-mPS and nPS were then diluted with phosphate-buffered saline depending on the appropriate volume of instillate (3  $\mu$ L per gram of mouse weight[24]). The radiochemical purity of the labeled product was determined by instant thin-layer chromatography with citric acid (0.1 M) in water as the mobile phase.

#### **In vitro stability**

An in vitro stability test was conducted for  $^{64}\text{Cu}$ -DOTA-mPS and  $^{64}\text{Cu}$ -DOTA-nPS by adding 3.08 MBq in 50  $\mu$ L to 200  $\mu$ L of mouse serum, simulated lung fluid (Biochemazone™), and phosphate-buffered saline (PBS). The samples were incubated at 37 °C for 72 h (until the end of the study period). At each time point, instant thin-layer chromatography (TLC) was performed with 0.1 M citric acid in water as the mobile phase to determine the percentage stability.

#### **Animal preparation and intratracheal instillation**

All animal experiments were performed in accordance with the institutional guidelines of the Korea Institute of Radiology and Medical Science (IACUC number: KIRAMS 2022–0079). C57BL/6 J mice (n=80; female, 8 weeks old; Shizuoka Laboratory Center, Japan) were used for the study and were allowed food pellets and water ad libitum during the entire course of the study. The mice were anesthetized via an intraperitoneal cocktail injection of ketamine hydrochloride (50–80 mg/kg body weight) and xylazine (8–12 mg/kg body weight). Once adequate anesthesia was observed by paw pinch stimulus, each mouse was fixed with its incisors to a rubber band on a board inclined at an angle of 45° to the lab bench. A mini laryngoscope (Hillrom™, USA) was used to clearly visualize the tracheal opening along with curved blunt-ended forceps to grasp the tongue, and the radioactive substance (after vortexing) was loaded into a 1-mL insulin syringe and gently instilled as an aerosol in the trachea by using an aerosol sprayer (Natsume Seisakusho, Tokyo, Japan) attached to the syringe. Post-instillation, the mice were monitored for breathing difficulty.

#### **PET/CT imaging**

Mice (n=5 per group) received intratracheal instillation of  $^{64}\text{Cu}$ -DOTA-mPS and/or nPS (1.1 MBq in 50  $\mu$ L) or  $^{64}\text{CuCl}_2$  (1.1 MBq in 50  $\mu$ L) for imaging. PET images were acquired 1, 12, 24, 48, and 72 h post-instillation. PET/CT image acquisition was performed on a Siemens Inveon PET Scanner (Siemens Medical Solutions, Germany) for 15 min per acquisition, with an energy window of 350–650 keV. Reconstruction of the acquired PET images was performed using the SP-MAP algorithm. The matrix size was 128×128×159, and the voxel size was 0.776×0.776×0.796 mm<sup>3</sup>.

For the acquisition of anatomical images, CT imaging was acquired with the second bed position, full rotation, and 180 projections per bed position. The exposure time was 200 ms, and the estimated scan time was 504 s. CT data were reconstructed using Feldkamp reconstruction with a Shepp–Logan filter. The effective pixel size of the reconstructed CT images was 109.69  $\mu$ m×109.69  $\mu$ m. PET and CT images were co-registered using the Inveon Research Workplace (Siemens Medical Solutions Inc.).

#### **Standard uptake value**

Region-of-interest analysis (ROI) to determine the uptake of the instilled tracer in major organs and tissues was performed using Inveon Research Workplace software (Siemens Medical Solutions Inc.). After co-registration of CT and PET data, the ROI was drawn on the CT image and copied to the PET data. A nuclear medicine expert drew the ROI after identifying the location in three cross-sectional images for precise ROI of the lungs, stomach, and liver (Additional file 3: Fig. S3-Additional file 5: Fig. S5). The maximal value within the ROI was used to avoid partial volume effects for the calculation of the standard uptake value (SUV).

#### **Biodistribution of $^{64}\text{Cu}$ -DOTA-polystyrene instilled mice**

Biodistribution was evaluated at 1, 12, 24, 48, and 72 h after intratracheal instillation of  $^{64}\text{Cu}$ -DOTA-mPS and/or nPS (n=5 at each time point) or  $^{64}\text{CuCl}_2$  (n=3 at each time point). Mice were euthanized, and major organs and blood were collected *in toto* while avoiding cross-contamination. Radioactivity was measured as counts per minute (CPM) in a WIZARDS2 Automatic  $\gamma$ -counter (PerkinElmer) and recorded in terms of percentage injected dose per gram of tissue (%ID/g).

#### **Ex vivo tissue-radio thin-layer chromatography (Ex vivo-radioTLC)**

To evaluate whether the counts recorded from the sample at 1 h post-instillation were from  $^{64}\text{Cu}$ -DOTA-mPS, nPS or  $^{64}\text{Cu}$ , ex vivo tissue-radio TLC was performed

with homogenized samples collected 1 h post-instillation. The tissues were homogenized using 10% SDS-PBS (pH 7.4), as described previously [10].

### Statistical analysis

The quantitative data obtained were expressed as mean  $\pm$  SD. Student's *t*-test was used to compare the means using PRISM software (GraphPad ver. 5.0, San Diego, CA, USA), and *P* values less than 0.05 were considered statistically significant.

## Results

### Chelation and radiolabeling

After radiolabeling, the purified  $^{64}\text{Cu}$ -DOTA-PS had a radiochemical purity of  $95.56\% \pm 0.31\%$  for mPS and  $94.21\% \pm 0.33\%$  for nPS, as determined by *ex vivo* radio instant thin layer chromatography (Additional file 1: Fig. S1A), and the radiolabeling yield was  $92.58\% \pm 0.7\%$  and  $50.67\% \pm 0.1\%$ , respectively.

DOTA conjugation was quantified using high-performance liquid chromatography (HPLC), and 690 nmol

and 630 nmol of DOTA were conjugated per milligram of mPS and nPS, respectively (Additional file 2: Fig. S2A). The scanning electron microscopy (SEM) data indicated that the diameter of polystyrene after DOTA conjugation was  $237.6 \text{ nm} \pm 5.1 \text{ nm}$  for mPS and  $21.6 \text{ nm} \pm 1.4 \text{ nm}$  for nPS, indicating negligible differences from the amino-polystyrene size prior to conjugation (Fig. 2).

### In vitro stability

The results of the *in vitro* stability test indicated that the labeled product was stable over the entire period of the study. The percentage stability of  $^{64}\text{Cu}$ -DOTA-mPS and  $^{64}\text{Cu}$ -DOTA-nPS in PBS (pH 7.4), simulated lung fluid, and mouse serum was shown in Additional file 1: Fig. S1B.

### Ex vivo tissue-radio thin-layer chromatography

The *ex vivo* iTLC performed for lungs, stomach and liver at 1 h confirmed that the counts from the organs belong to  $^{64}\text{Cu}$ -DOTA-mPS/nPS and not  $^{64}\text{Cu}$  proving that the labelled product is stable *in vivo*. The results are shown

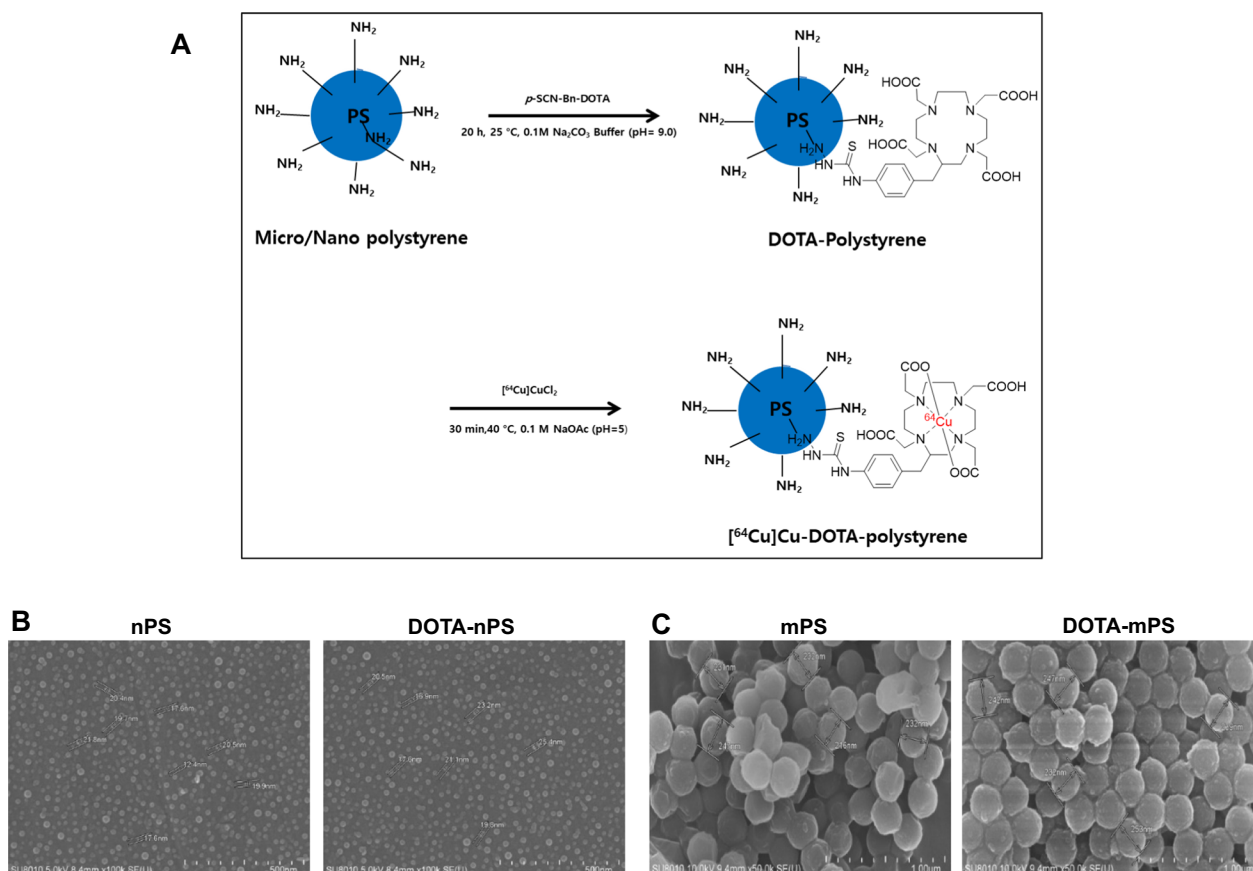


**Fig. 2** Radiolabelling of  $^{64}\text{Cu}$ -DOTA-polystyrene and characterization of DOTA-mPS and DOTA-nPS using field emission scanning electron microscope. **(A)** Conjugation of DOTA with polystyrene under specific conditions. **(B)** Field emission scanning electron microscope results show no difference between polystyrene bead and DOTA-polystyrene bead of both sizes (mPS = micro-polystyrene, nPS = nano-polystyrene)

in Additional file 2: Fig. S2B. It was ensured that there was no de-chelation of the radio-labelled PS in the stomach due to the acidic environment by *ex-vivo* instant thin-layer chromatography (iTLC) and the results confirmed that the  $^{64}\text{Cu}$ -DOTA-mPS/nPS was intact at 1 h. The *ex-vivo* iTLC results shown in Additional file 2: Fig. S2B explains that the radioactivity emanating from the organs are from the  $^{64}\text{Cu}$ -DOTA-mPS/nPS and not from  $^{64}\text{Cu}$  since the labelled product remains at origin and  $^{64}\text{Cu}$  travels to the solvent front in TLC when 0.1 M citric acid is used as mobile phase [25].

### PET imaging

PET imaging was performed until 72 h post-intratracheal instillation of  $^{64}\text{Cu}$ -DOTA-mPS and/or nPS or  $^{64}\text{CuCl}_2$  along with a biodistribution study at the set time points. The acquired sequential PET/CT images are presented in Fig. 3A and Additional file 3: Fig. S3. Quantitative data

obtained in terms of  $\text{SUV}_{\text{max}}$  for the lungs, stomach, and liver were plotted against time (Fig. 3B).

The PET images clearly indicated the presence of  $^{64}\text{Cu}$ -DOTA-mPS within the lungs (marked “L” in Fig. 3A) for up to 72 h, with an  $\text{SUV}_{\text{max}}$  of  $11.7 \pm 5.0$ ,  $48.3 \pm 6.2$ ,  $65.5 \pm 2.3$ ,  $42.2 \pm 13.1$ , and  $13.2 \pm 2.3$  at 1, 12, 24, 48, and 72 h, respectively. These values were significantly different from those for  $^{64}\text{CuCl}_2$  and  $^{64}\text{Cu}$ -DOTA-nPS at all time points after 12 h. The AUC-lung for  $^{64}\text{Cu}$ -DOTA-mPS was 10.84-fold and 3.47-fold that of  $^{64}\text{Cu}$  and  $^{64}\text{Cu}$ -DOTA-nPS, respectively (Fig. 3B).

However, slight transit of the radiolabeled mPS from the instilled location in the trachea into the stomach was observed in the initial 1 h image, which then decreased substantially in the later images, with  $\text{SUV}_{\text{max}}$  values of  $13.0 \pm 2.7$ ,  $9.2 \pm 0.7$ ,  $7.1 \pm 2.5$ ,  $2.8 \pm 0.6$ , and  $2.0 \pm 0.5$  at 1, 12, 24, 48, and 72 h, respectively, in the stomach. Furthermore, radioactivity was observed in the liver, which

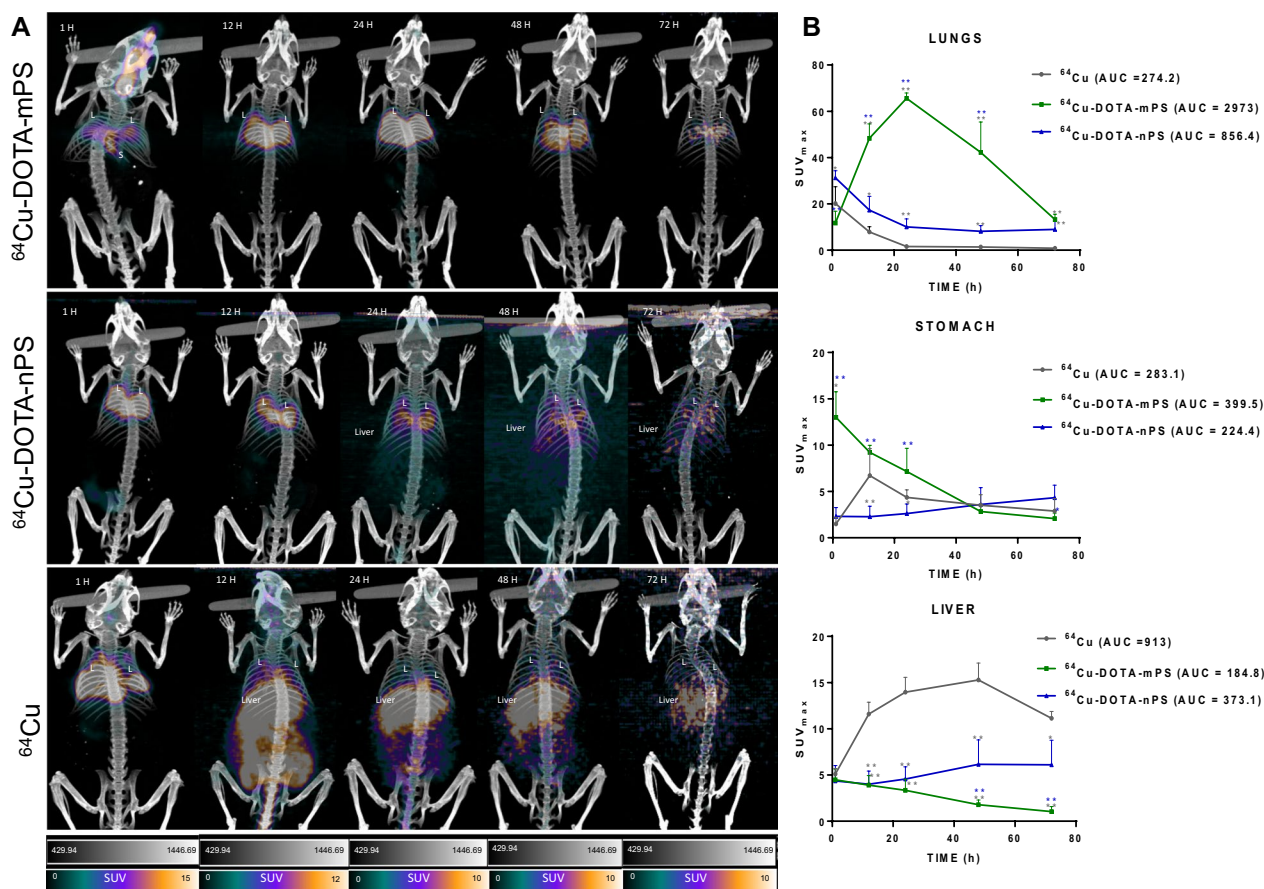


**Fig. 3** (A) Representative PET-CT images of intra-tracheally instilled  $^{64}\text{Cu}$ -DOTA-mPS,  $^{64}\text{Cu}$ -DOTA-nPS and  $^{64}\text{Cu}$  at all time points displaying retention of polystyrene in lungs compared to  $^{64}\text{Cu}$  that is rapidly cleared from the lungs post instillation. (B) The graphs represent  $\text{SUV}_{\text{max}}$  for important organs such as lungs, stomach and liver along with the AUC which is maximum for mPS in lungs and  $^{64}\text{Cu}$  in liver. AUC = area under curve; mPS = micro-polystyrene; nPS = nano-polystyrene; L = lungs; S = stomach (\* $P < 0.05$ , \*\* $P < 0.005$ , \* significance in comparison to  $^{64}\text{Cu}$ ; \* significance in comparison to  $^{64}\text{Cu}$ -DOTA-nPS)

decreased gradually over time with  $SUV_{max}$  values of  $4.4 \pm 1.1$ ,  $3.9 \pm 1.0$ ,  $3.3 \pm 1.2$ ,  $1.7 \pm 0.5$ , and  $1.0 \pm 0.5$  at 1, 12, 24, 48, and 72 h, respectively.

The PET of  $^{64}Cu$ -DOTA-nPS exhibited a different pattern, with maximum activity and a markedly elevated  $SUV_{max}$  observed in the lung (marked “L” in Fig. 3A) post-instillation. The lungs showed  $SUV_{max}$  values of  $31.2 \pm 3.1$ ,  $17.3 \pm 5.9$ ,  $10.0 \pm 3.4$ ,  $8.1 \pm 2.4$ , and  $8.9 \pm 3.6$  at 1, 12, 24, 48, and 72 h, respectively. Although the radioactivity observed in the stomach was not as high as that in the  $^{64}Cu$ -mPS group, some  $^{64}Cu$ -DOTA-nPS radioactivity was observed in the stomach, with  $SUV_{max}$  values of  $2.3 \pm 0.9$ ,  $2.2 \pm 1.1$ ,  $2.6 \pm 1.0$ ,  $3.6 \pm 1.8$ , and  $4.3 \pm 1.3$  at 1, 12, 24, 48, and 72 h, respectively. The liver accumulated the radiolabeled nPS gradually post-instillation, with an  $SUV_{max}$  of  $6.1 \pm 2.6$  at 72 h.

In the  $^{64}Cu$ -instilled mice, radioactivity was distributed instantly into the entire lungs after intratracheal instillation, and less uptake was detected in the stomach, unlike in the radiolabeled mPS-instilled group. However, activity in the lungs was translocated relatively early. The  $SUV_{max}$  in the lungs was  $20.1 \pm 7.2$  at 1 h post-instillation, after which it decreased rapidly to  $7.8 \pm 2.2$  at 12 h,  $1.6 \pm 0.5$  at 24 h,  $1.4 \pm 0.1$  at 48 h, and  $0.85 \pm 0.20$  at 72 h.  $^{64}Cu$  activity, however, accumulated in the liver (marked “Liver” in Fig. 3A) in the initial image at 1 h, possibly as a result of  $^{64}Cu$  crossing the air–blood barrier (ABB) into the blood circulation and sequestering by the liver [25]. The  $SUV_{max}$  values in the liver were  $5.1 \pm 0.6$ ,  $11.6 \pm 1.2$ ,  $13.9 \pm 1.6$ ,  $15.2 \pm 1.8$ , and  $11.1 \pm 0.7$  at 1, 12, 24, 48, and 72 h, respectively (Fig. 3B,  $*P < 0.05$ ,  $**P < 0.005$ ). Moreover, the AUC-liver was 4.94-fold and 2.44-fold that for  $^{64}Cu$ -DOTA-mPS and  $^{64}Cu$ -DOTA-nPS, respectively. Additionally, observable uptake was noted in the small intestine, large intestine, kidney, and urinary bladder.

### Biodistribution

Interestingly, the distribution pattern from the biodistribution data (Fig. 4) was similar to that observed in the PET images. The  $\gamma$ -counting data were consistent with the PET/CT scan data, and the mean %ID/g of  $^{64}Cu$ -DOTA-mPS in the lungs was significantly higher than that of  $^{64}Cu$  and  $^{64}Cu$ -DOTA-nPS at 72 h post-instillation (Fig. 4,  $*P < 0.05$ ,  $**P < 0.005$ ).

The lung retention of  $^{64}Cu$ -DOTA-nPS was lower than that of  $^{64}Cu$ -DOTA-mPS, but 3.9-fold higher than the mean %ID/g of  $^{64}Cu$  at 72 h. However, the mean %ID/g of  $^{64}Cu$ -DOTA-nPS in the liver was considerably greater after 72 h, being 9.9-fold that of  $^{64}Cu$ -DOTA-mPS. But the %ID/g of  $^{64}Cu$ -DOTA-nPS was 1.56-fold lower than the %ID/g of  $^{64}Cu$  in the liver at 72 h.

On the other hand, the  $^{64}Cu$ -instilled group showed almost complete clearance from lungs (%ID/g  $3.6\% \pm$

$3.2\%$  at 72 h;  $*P < 0.05$ ,  $**P < 0.005$ ) as well as the highest liver uptake among all the three groups at all time points, which gradually increased post-instillation until 48 h, indicating the translocation of  $^{64}Cu$  from the lungs by crossing the ABB. The %ID/g for the liver in the  $^{64}Cu$  group was  $10.6 \pm 6.9\%$ ,  $13.1 \pm 2.0\%$ ,  $14.8 \pm 14.2\%$ ,  $23.2 \pm 8.7\%$ , and  $18.1 \pm 6.2\%$  at 1, 12, 24, 48, and 72 h.

In addition, we identified the uptake of radiolabeled mPS and nPS in the circulatory systems such as blood, heart, spleen, and gastro-intestinal system such as liver, intestine, and the other organs such as thymus, lymph node, kidney, salivary glands, urinary bladder, and even to brain. The mean %ID/g of  $^{64}Cu$ -DOTA-nPS in brain was 2.26-fold higher than mPS and %ID/g of  $^{64}Cu$ -DOTA-nPS in spleen was 3.12-fold higher than  $^{64}Cu$  at 72 h ( $*P < 0.05$ ,  $**P < 0.005$ ). By the end-point, blood had increased uptake of  $^{64}Cu$  (%ID/g  $2.20\% \pm 0.68\%$ ) followed by nPS (%ID/g  $1.60\% \pm 0.55\%$ ) and then mPS (%ID/g  $0.50\% \pm 0.33\%$ ). Though not significant, the mean %ID/g of  $^{64}Cu$ -DOTA-nPS at 72 h was higher than that of mPS in thymus, kidneys, salivary glands, ovaries, and urinary bladder.

### Discussion

To the best of our knowledge, we first revealed the in vivo biodistribution of mPS and nPS after intratracheal instillation in mice using PET and ex vivo biodistribution assays using  $\gamma$ -counter. In our study, PET imaging, and post-mortem organ biodistribution data indicated that  $^{64}Cu$ -DOTA-mPS primarily remained within the lungs of mice for up to 72 h after instillation. Although the radioactivity gradually decreased over time, the %ID/g in the lungs at 72 h in mice that received instillation of  $^{64}Cu$ -DOTA-mPS was significantly higher than that in mice receiving  $^{64}Cu$ .  $^{64}Cu$ -DOTA-nPS also showed retention of radioactivity within the lungs, but most of the nPS was cleared off rapidly in comparison with the corresponding findings for mPS. We identified higher accumulation of %ID/g for nPS (roughly 2 times) compared to mPS in spleen, liver, small and large intestine, thymus, kidney, brain, salivary gland, ovary, and urinary bladder at 72 h after intratracheal instillation (Fig. 4).

Fast clearance of nPS compared to mPS in lung would be possibly because nPS may easily cross the ABB into the systemic circulation from the alveolar region [26]. Mode of elimination involves the transfer into the pulmonary lymph nodes after phagocytosis by alveolar macrophages [27, 28], which is a prominent clearance mechanism in the alveolar region, especially for insoluble particles. Similarly, ultrafine particles such as  $PM_{0.1}$  (particles less than 100 nm in diameter) could enter the bloodstream by dissolving rapidly in the lipid and/or the fluid lining the alveolar wall [29]. Uptake into the bloodstream and

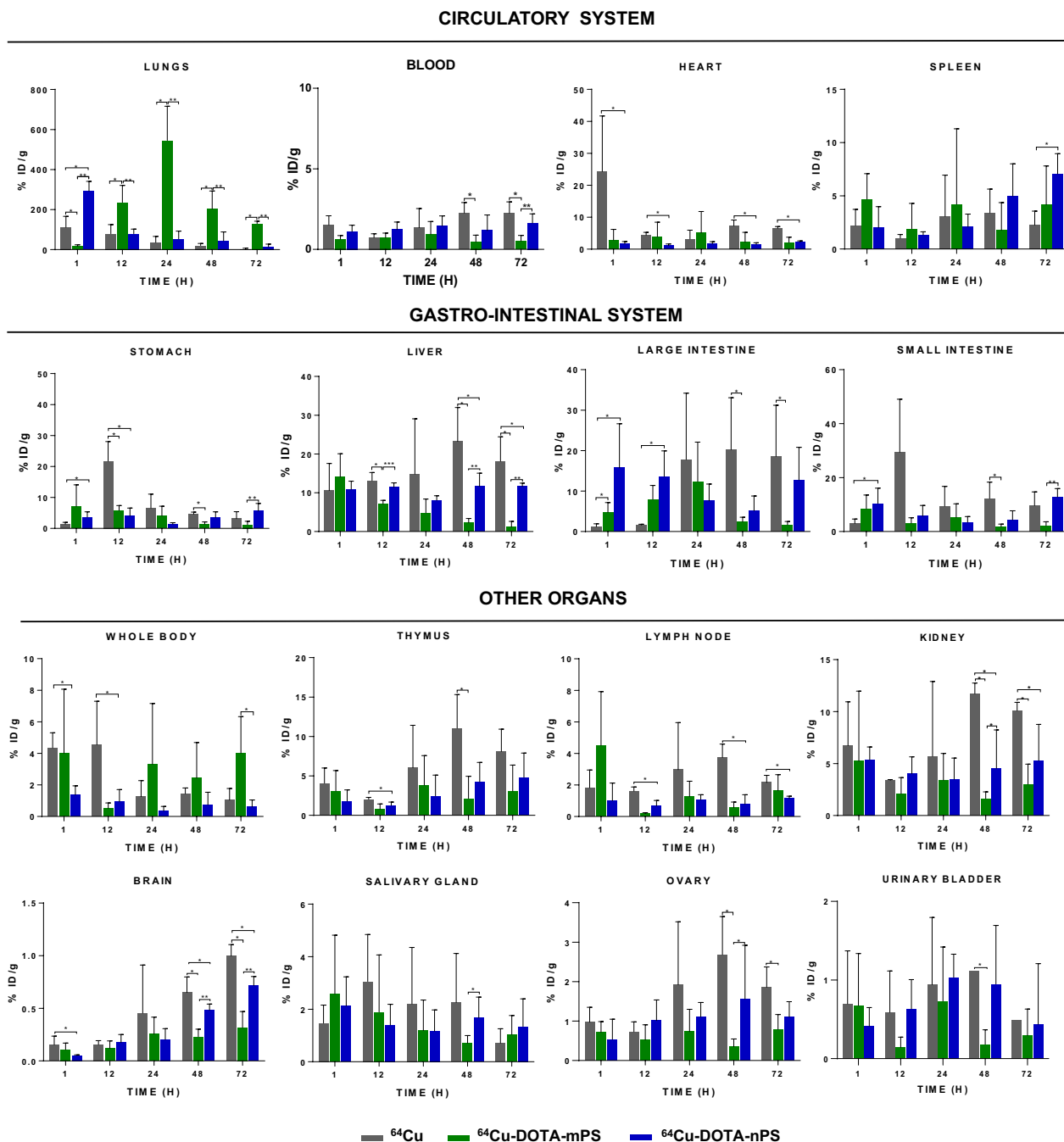


**Fig. 4** Bio-distribution data of the intra-tracheally instilled <sup>64</sup>Cu-DOTA-mPS (n=5), <sup>64</sup>Cu-DOTA-nPS (n=5) and <sup>64</sup>Cu (n=3) groups for all organ systems. The instilled radioactivity can be seen distributed to various organs especially stomach, small intestine, large intestine, liver, spleen, kidneys, and thymus. The data suggests that <sup>64</sup>Cu subsequently crossed the ABB in the lungs and got accumulated in the liver by 12 h and also in other organs in small amounts. However, mPS and nPS retained in the lungs and cleared slowly as compared to <sup>64</sup>Cu. Faster clearance from the lungs to other organs like liver can be noted in nPS data as compared to the mPS bio-distribution results. The %ID/g in the lung for mPS was significantly different than that of <sup>64</sup>Cu and nPS at all time points. mPS= micro-polystyrene; nPS= nano-polystyrene. (\*P < 0.05, \*\*P < 0.005, \*\*\*P < 0.0005 Student t test)



lymphatics occurs in the interstitium via diffusion. Fast translocation into the ABB could be explained by following processes: (a) cell-mediated active transportation, (b) passive transportation such as diffusion, and (c) active or passive transportation through the pores in the endothelial cells or gaps between the alveolar epithelial cells [30]. Further, the differences in the rate of clearance can be explained on the basis of the modes of elimination, since larger-sized plastics (mPS in this study) are phagocytosed by alveolar macrophages and eliminated by the mucociliary apparatus or remain in the lung interstitium, whereas smaller plastics (nPS in this study) may enter the blood capillaries [30]. The pharmacokinetics of PS may differ depending on the modification properties, such as the size and surface chemistry, and it may affect in vivo behavior once it enters the systemic circulation. Molecular weight and sizes play important roles in the clearance mechanism [31]. Renal and hepatic clearance play important roles in the elimination of nano- and micro-sized particles from the circulatory system [32]. Consistent with these findings,  $^{64}\text{Cu}$ -DOTA-mPS/nPS were also taken up by the liver or excreted through the renal route. Liver and spleen uptake can be explained as a function of the reticuloendothelial system (RES) to phagocytose mPS and nPS in the systemic circulation. The uptake of nPS in the liver increased, similar to the uptake of  $^{64}\text{Cu}$ , however, the distribution of  $^{64}\text{Cu}$ -DOTA-nPS observed in other organs were different in comparison to  $^{64}\text{Cu}$ . Whereas, the %ID/g of  $^{64}\text{Cu}$ -DOTA-mPS in the liver was high only at the initial time point and then decreased gradually. Our previous study on the oral administration of  $^{64}\text{Cu}$ -DOTA-mPS also revealed liver activity [10]. The %ID/g of  $^{64}\text{Cu}$ -DOTA-mPS and/or nPS in the brain increased gradually post-instillation. The blood–brain barrier (BBB) consists of brain endothelial cells attached to the basement membrane and linked together by tight junctions, and even small-molecule drugs can barely cross the BBB due to these properties [33]. Therefore, the absolute value of  $^{64}\text{Cu}$ -DOTA-PS brain uptake was less and size-dependent; thus, the nPS concentration was higher than that of mPS. Previously, we reported ingested polyethylene would be as possible risk factor for autism spectrum disorder [8]. According to these findings in this study, nPS may be more likely to damage the brain than mPS, which requires further longitudinal research.

The stomach, liver, and intestine were not clearly visible from Fig. 3A and Additional file 3: Fig. S3 due to large differences of PET intensity. However, after window adjustment, higher uptake in the trachea and lungs were saturated and then PET uptake in stomach, liver, and intestine could be clearly visible (Additional file 4: Fig. S4, Additional file 5: S5). Higher stomach activity was observed in the mPS group immediately post-instillation.

Here, PET uptake in the stomach could be explained due to the muco-ciliary clearance mechanism in the respiratory tract. Several studies involving bio-distribution of intra-tracheally instilled radioisotope labelled particles had shown stomach uptake as well [34, 35]. Muco-ciliary clearance was observed when  $\text{PM}_{10}$  (particles less than  $10\ \mu\text{m}$  in diameter) were deposited in the trachea [36]. The muco-ciliary mechanism of the respiratory system plays a major role in the elimination of inhaled particles by subsequent ingestion into the gastrointestinal system and excretion through the bowels [37, 38]. Muco-ciliary clearance is the primary innate defense mechanism of the lungs, and it involves the mucous layer, airway surface liquid layer, and cilia. These cilia can propel the particles trapped in the mucous layer after inhalation. At the pharynx, these particles mix with salivary secretions and enter the gastrointestinal tract due to swallowing [31, 37]. Following this mechanism, it was evident that nPS and  $^{64}\text{Cu}$  were accumulated in the liver by fast clearance from lungs as they might have possibly crossed ABB into the systemic circulation where mPS being larger in size retained in the lungs over longer time interval following muco-ciliary clearance as evident from the increased stomach uptake in mPS post-instillation.

The amount of  $^{64}\text{Cu}$ -DOTA-mPS retained within the lung was significantly higher than that of  $^{64}\text{Cu}$ -DOTA-nPS. Therefore, mPS might possibly induce higher toxicity in the lung. However, the amount of  $^{64}\text{Cu}$ -DOTA-nPS retained was significantly higher than that of  $^{64}\text{Cu}$ -DOTA-mPS in other organs such as spleen, liver, small and large intestine, thymus, kidney, brain, salivary gland, ovary, and urinary bladder, indicating that longitudinal and chronic exposure of nPS may induce more hazardous effects to these organs compared to mPS.

Limitation of this study was spillover effect on PET due to the limited spatial resolution. Although spillover effect was contributed,  $\text{SUV}_{\text{max}}$  and %ID/g values showed a similar pattern or trend.

Taken together, our results demonstrated the utility of PET for visualizing the absorption and distribution of mPS and nPS radiolabeled with  $^{64}\text{Cu}$ . PET provides information on the accumulation of mPS and nPS in vivo and can provide information on how each organ could be affected following continuous mPS and nPS inhalation. The biological effects of long-term exposure to mPS and nPS in each organ affected in this study will be evaluated in future studies.

## Conclusion

We traced inhaled mPS and/or nPS using  $^{64}\text{Cu}$  labeling technique and PET imaging. We showed that the accumulated amount of mPS or nPS between lungs and other interesting organs were different depending on the size of

PS. These findings would be the basis for future toxicity studies on each organ in the future, which requires longitudinal evaluations of toxicity.

## Supplementary Information

The online version contains supplementary material available at <https://doi.org/10.1186/s12989-023-00561-7>.

- Additional file 1: Fig. S1.** Radiochemical purity and In-vitro stability
- Additional file 2: Fig. S2.** HPLC data and Ex-vivo TLC of organs
- Additional file 3: Fig. S3.** The transverse, coronal and sagittal PET images
- Additional file 4: Fig. S4.** PET representative images
- Additional file 5: Fig. S5.** PET representative images

### Author contributions

Conceptualization, J. S. K.; writing-original draft preparation, J.S.; writing-review and editing, J. S. K.; Funding acquisition, J. S. K.; Proofreading-J.S.K.; Experimental work, Z. J. C.I.; Data analysis, C.M.K.

### Funding

This work was supported partly by Program Ministry of Science and ICT (No. NRF- 2021M2E8A1039980, 50461-2023, 50462-2023), partly by Korea Environment Industry & Technology Institute (KEITI) through Measurement and Risk assessment Program for Management of Microplastics Program, funded by Korea Ministry of Environment (MOE) (RS-2022-KE002132).

### Availability of data and materials

For data sharing: please contact [kjs@kirams.re.kr](mailto:kjs@kirams.re.kr).

### Declarations

#### Ethical approval and consent to participate

All animal experiments were performed in accordance with the institutional guidelines of the Korea Institute of Radiological and Medical Sciences (KIRAMS) and the protocols were approved by the Institutional Animal Care and Use Committee (IACUC number: KIRAMS 2022-0079).

#### Consent for publication

All authors have consented for publication.

#### Competing interests

The authors declare no conflicts of interest. The funders had no role in the design of the study, in the collection, analyses, or interpretation of data, in the writing of the manuscript, or in the decision to publish the results.

#### Author details

<sup>1</sup>Division of RI Application, Korea Institute of Radiological and Medical Sciences, 75 Nowon-Gil, Gongneung-Dong, Nowon-Gu, Seoul 01812, Korea.

<sup>2</sup>Radiological and Medico-Oncological Sciences, Korea National University of Science and Technology, Seoul 01812, Republic of Korea.

Received: 18 September 2023 Accepted: 24 December 2023

Published online: 31 January 2024

## References

- Mallory ML, Baak J, Gjerdrum C, Mallory OE, Manley B, Swan C, et al. Anthropogenic litter in marine waters and coastlines of Arctic Canada and West Greenland. *Sci Total Environ.* 2021;783:146971. <https://doi.org/10.1016/j.scitotenv.2021.146971>.
- Peng L, Fu D, Qi H, Lan CQ, Yu H, Ge C. Micro- and nano-plastics in marine environment: Source, distribution and threats—a review. *Sci Total Environ.* 2020;698:134254. <https://doi.org/10.1016/j.scitotenv.2019.134254>.
- Jenner LC, Rotchell JM, Bennett RT, Cowen M, Tentzeris V, Sadofsky LR. Detection of microplastics in human lung tissue using  $\mu$ FTIR spectroscopy. *Sci Total Environ.* 2022;831:154907. <https://doi.org/10.1016/j.scitotenv.2022.154907>.
- Kannan K, Vimalkumar K. A Review of Human Exposure to Microplastics and Insights Into Microplastics as Obesogens. *Front Endocrinol (Lausanne).* 2021;12:724989. <https://doi.org/10.3389/fendo.2021.724989>.
- Kik K, Bukowska B, Sicińska P. Polystyrene nanoparticles: Sources, occurrence in the environment, distribution in tissues, accumulation and toxicity to various organisms. *Environ Pollut.* 2020;262:114297. <https://doi.org/10.1016/j.envpol.2020.114297>.
- Kim H, Zaheer J, Choi EJ, Kim JS. Enhanced ASGR2 by microplastic exposure leads to resistance to therapy in gastric cancer. *Theranostics.* 2022;12(7):3217–36. <https://doi.org/10.7150/thno.73226>.
- Tong X, Li B, Li J, Li L, Zhang R, Du Y, et al. Polyethylene microplastics cooperate with *Helicobacter pylori* to promote gastric injury and inflammation in mice. *Chemosphere.* 2022;288(Pt 2):132579. <https://doi.org/10.1016/j.chemosphere.2021.132579>.
- Zaheer J, Kim H, Ko IO, Jo EK, Choi EJ, Lee HJ, et al. Pre/post-natal exposure to microplastic as a potential risk factor for autism spectrum disorder. *Environ Int.* 2022;161:107121. <https://doi.org/10.1016/j.envint.2022.107121>.
- Zhao J, Gomes D, Jin L, Mathis SP, Li X, Rouchka EC, et al. Polystyrene bead ingestion promotes adiposity and cardiometabolic disease in mice. *Ecotoxicol Environ Saf.* 2022;232:113239. <https://doi.org/10.1016/j.ecoenv.2022.113239>.
- Im C, Kim H, Zaheer J, Kim JY, Lee YJ, Kang CM, et al. PET Tracing of Biodistribution for Orally Administered (64)Cu-Labeled Polystyrene in Mice. *J Nucl Med.* 2022;63(3):461–7. <https://doi.org/10.2967/jnumed.120.256982>.
- da Silva Brito WA, Mutter F, Wende K, Cecchini AL, Schmidt A, Bekeschus S. Consequences of nano and microplastic exposure in rodent models: the known and unknown. *Part Fibre Toxicol.* 2022;19(1):28. <https://doi.org/10.1186/s12989-022-00473-y>.
- Lai H, Liu X, Qu M. Nanoplastics and Human Health: Hazard Identification and Biointerface. *Nanomaterials (Basel).* 2022. <https://doi.org/10.3390/nano12081298>.
- Rodrigues ACB, de Jesus GP, Waked D, Gomes GL, Silva TM, Yariwake VY, et al. Scientific evidence about the risks of micro and nanoplastics (MNPLs) to human health and their exposure routes through the environment. *Toxics.* 2022. <https://doi.org/10.3390/toxics10060308>.
- Lim X. Microplastics are everywhere—But are they harmful? *Nature.* 2021;593(7857):22–5. <https://doi.org/10.1038/d41586-021-01143-3>.
- Amato-Lourenço LF, Carvalho-Oliveira R, Júnior GR, Dos Santos GL, Ando RA, Mauad T. Presence of airborne microplastics in human lung tissue. *J Hazard Mater.* 2021;416:126124. <https://doi.org/10.1016/j.jhazmat.2021.126124>.
- Kwon JH, Kim JW, Pham TD, Tarafdar A, Hong S, Chun SH, et al. Microplastics in food: a review on analytical methods and challenges. *Int J Environ Res Public Health.* 2020;17(18):6710. <https://doi.org/10.3390/ijerph17186710>.
- Rubio-Armendáriz C, Alejandro-Vega S, Paz-Montelongo S, Gutiérrez-Fernández AJ, Carrascosa-Iruzebieta CJ, la Hardisson-de Torre A. Microplastics as emerging food contaminants: a challenge for food safety. *Int J Environ Res Public Health.* 2022. <https://doi.org/10.3390/ijerph19031174>.
- Sánchez A, Rodríguez-Viso P, Domene A, Orozco H, Vélez D, Devesa V. Dietary microplastics: occurrence, exposure and health implications. *Environ Res.* 2022;212(Pt A):113150. <https://doi.org/10.1016/j.envres.2022.113150>.
- Ageel HK, Harrad S, Abdallah MA. Occurrence, human exposure, and risk of microplastics in the indoor environment. *Environ Sci Process Impacts.* 2022;24(1):17–31. <https://doi.org/10.1039/d1em00301a>.
- Enyoh CE, Verla AW, Verla EN, Ibe FC, Amaobi CE. Airborne microplastics: a review study on method for analysis, occurrence, movement and risks. *Environ Monit Assess.* 2019;191(11):668. <https://doi.org/10.1007/s10661-019-7842-0>.
- Rahman L, Mallach G, Kulka R, Halappanavar S. Microplastics and nanoplastics science: collecting and characterizing airborne microplastics in fine particulate matter. *Nanotoxicology.* 2021;15(9):1253–78. <https://doi.org/10.1080/17435390.2021.2018065>.

22. Huang Y, Wong KK, Li W, Zhao H, Wang T, Stanescu S, et al. Characteristics of nano-plastics in bottled drinking water. *J Hazard Mater.* 2022;424(Pt C): 127404. <https://doi.org/10.1016/j.jhazmat.2021.127404>.
23. Wadas TJ, Wong EH, Weisman GR, Anderson CJ. Coordinating radiometals of copper, gallium, indium, yttrium, and zirconium for PET and SPECT imaging of disease. *Chem Rev.* 2010;110(5):2858–902. <https://doi.org/10.1021/cr900325h>.
24. Helms MN, Torres-Gonzalez E, Goodson P, Rojas M. Direct tracheal instillation of solutes into mouse lung. *J Vis Exp.* 2010. <https://doi.org/10.3791/1941>.
25. Wang H, Chen X. Visualization of copper metabolism by  $^{64}\text{CuCl}_2$ -PET. *Mol Imaging Biol.* 2012;14(1):14–6. <https://doi.org/10.1007/s11307-011-0483-5>.
26. Wooten AL, Aweda TA, Lewis BC, Gross RB, Lapi SE. Biodistribution and PET Imaging of pharmacokinetics of manganese in mice using Manganese-52. *PLoS ONE.* 2017;12(3):e0174351. <https://doi.org/10.1371/journal.pone.0174351>.
27. Nagre N, Cong X, Pearson AC, Zhao X. Alveolar macrophage phagocytosis and bacteria clearance in mice. *J Vis Exp.* 2019. <https://doi.org/10.3791/59088>.
28. Allard B, Panariti A, Martin JG. Alveolar macrophages in the resolution of inflammation, tissue repair, and tolerance to infection. *Front Immunol.* 2018;9:1777. <https://doi.org/10.3389/fimmu.2018.01777>.
29. Schraufnagel DE. The health effects of ultrafine particles. *Exp Mol Med.* 2020;52(3):311–7. <https://doi.org/10.1038/s12276-020-0403-3>.
30. Shimada A, Kawamura N, Okajima M, Kaewamatawong T, Inoue H, Morita T. Translocation pathway of the intratracheally instilled ultrafine particles from the lung into the blood circulation in the mouse. *Toxicol Pathol.* 2006;34(7):949–57. <https://doi.org/10.1080/01926230601080502>.
31. Sakoda A, Ishimori Y, Fukao K, Yamaoka K, Kataoka T, Mitsunobu F. Lung dosimetry of inhaled radon progeny in mice. *Radiat Environ Biophys.* 2012;51(4):425–42. <https://doi.org/10.1007/s00411-012-0431-z>.
32. Simon BH, Ando HY, Gupta PK. Circulation time and body distribution of  $^{14}\text{C}$ -labeled amino-modified polystyrene nanoparticles in mice. *J Pharm Sci.* 1995;84(10):1249–53. <https://doi.org/10.1002/jps.2600841020>.
33. Abbott NJ, Patabendige AA, Dolman DE, Yusof SR, Begley DJ. Structure and function of the blood-brain barrier. *Neurobiol Dis.* 2010;37(1):13–25. <https://doi.org/10.1016/j.nbd.2009.07.030>.
34. Mao L, Hu M, Pan B, Xie Y, Petersen EJ. Biodistribution and toxicity of radio-labeled few layer graphene in mice after intratracheal instillation. *Part Fibre Toxicol.* 2016;13:7. <https://doi.org/10.1186/s12989-016-0120-1>.
35. Park JE, Lee JY, Chae J, Min CH, Shin HS, Lee SY, et al. In vivo tracking of toxic diesel particulate matter in mice using radiolabeling and nuclear imaging. *Chemosphere.* 2023;313:137395. <https://doi.org/10.1016/j.chemosphere.2022.137395>.
36. Leikauf GD, Kim SH, Jang AS. Mechanisms of ultrafine particle-induced respiratory health effects. *Exp Mol Med.* 2020;52(3):329–37. <https://doi.org/10.1038/s12276-020-0394-0>.
37. Bustamante-Marin XM, Ostrowski LE. Cilia and mucociliary clearance. *Cold Spring Harb Perspect Biol.* 2017. <https://doi.org/10.1101/cshperspect.a028241>.
38. Hofmann W, Asgharian B. The effect of lung structure on mucociliary clearance and particle retention in human and rat lungs. *Toxicol Sci.* 2003;73(2):448–56. <https://doi.org/10.1093/toxsci/kfg075>.

## Publisher's Note

Springer Nature remains neutral with regard to jurisdictional claims in published maps and institutional affiliations.